Pr and F co-doped SnO_2 transparent conductive films with high work function deposited by ion-assisted electron beam evaporation

Shaohang Wu,[1,2] Yantao Li,[1] Jinsong Luo,[1] Jie Lin,[1] Yi Fan,[1,3] Zhihong Gan,[1] and Xingyuan Liu[1,*]

[1]*State Key Laboratory of Luminescence and Applications, Changchun Institute of Optics, Fine Mechanics and Physics, Chinese Academy of Sciences, Changchun 130033, China*
[2]*University of Chinese Academy of Sciences, Beijing 100049, China*
[3]*fanyi@ciomp.ac.cn*
[*]*liuxy@ciomp.ac.cn*

Abstract: A transparent conductive oxide (TCO) Pr and F co-doped SnO_2 (PFTO) film is prepared by ion-assisted electron beam deposition. An optimized PFTO film shows a high average visible optical transmittance of 83.6% and a minimum electrical resistivity of 3.7×10^{-3} Ω·cm corresponding to a carrier density of 1.298×10^{20} cm^{-3} and Hall mobility of 12.99 $cm^2/V{\cdot}s$. This PFTO film shows a high work function of 5.147 eV and favorable surface morphology with an average roughness of 1.45 nm. Praseodymium fluoride is found to be an effective material to dope F into SnO_2 that can simplify the fabrication process of SnO_2-based TCO films.

OCIS codes: (310.7005) Transparent conductive coatings; (310.6845) Thin film devices and applications.

References and links

1. D. S. Ginley and C. Bright, "Transparent conducting oxides," MRS Bull. **25**(08), 15–18 (2000).
2. S. Ito, T. N. Murakami, P. Comte, P. Liska, C. Grätzel, M. K. Nazeeruddin, and M. Grätzel, "Fabrication of thin film dye sensitized solar cells with solar to electric power conversion efficiency over 10%," Thin Solid Films **516**(14), 4613–4619 (2008).
3. T. Minami, "Transparent conducting oxide semiconductors for transparent electrodes," Semicond. Sci. Technol. **20**(4), S35–S44 (2005).
4. H. B. Li, N. Wang, and X. Y. Liu, "Optical and electrical properties of Vanadium doped Indium oxide thin films," Opt. Express **16**(1), 194–199 (2008).
5. N. Wang, X. X. Liu, and X. Y. Liu, "Ultraviolet luminescent, high-effective-work-function $LaTiO_3$-doped indium oxide and its effects in organic optoelectronics," Adv. Mater. **22**(19), 2211–2215 (2010).
6. Y. Q. Liao, Q. P. Lu, Y. Fan, and X. Y. Liu, "Manganese-doped indium oxide and its application in organic light-emitting diodes," Appl. Phys. Lett. **99**(2), 023302 (2011).
7. M. G. Helander, Z. B. Wang, J. Qiu, M. T. Greiner, D. P. Puzzo, Z. W. Liu, and Z. H. Lu, "Chlorinated indium tin oxide electrodes with high work function for organic device compatibility," Science **332**(6032), 944–947 (2011).
8. D. S. Hecht, L. Hu, and G. Irvin, "Emerging transparent electrodes based on thin films of carbon nanotubes, graphene, and metallic nanostructures," Adv. Mater. **23**(13), 1482–1513 (2011).
9. Y. Park, V. Choong, Y. Gao, B. Hsieh, and C. W. Tang, "Work function of indium tin oxide transparent conductor measured by photoelectron spectroscopy," Appl. Phys. Lett. **68**(19), 2699–2701 (1996).
10. V. I. Adamovich, S. R. Cordero, P. I. Djurovich, A. Tamayo, M. E. Thompson, B. W. D'Andrade, and S. R. Forrest, "New charge-carrier blocking materials for high efficiency OLEDs," Org. Electron. **4**(2–3), 77–87 (2003).
11. M. T. Greiner, M. G. Helander, W. M. Tang, Z. B. Wang, J. Qiu, and Z. H. Lu, "Universal energy-level alignment of molecules on metal oxides," Nat. Mater. **11**(1), 76–81 (2012).
12. D. Milliron, I. Hill, C. Shen, A. Kahn, and J. Schwartz, "Surface oxidation activates indium tin oxide for hole injection," J. Appl. Phys. **87**(1), 572–576 (2000).
13. I. D. Parker, "Carrier tunneling and device characteristics in polymer light-emitting diodes," J. Appl. Phys. **75**(3), 1656–1666 (1994).
14. G. Malliaras and J. Scott, "The roles of injection and mobility in organic light emitting diodes," J. Appl. Phys. **83**(10), 5399–5403 (1998).

#200209 - $15.00 USD Received 25 Oct 2013; revised 1 Feb 2014; accepted 16 Feb 2014; published 21 Feb 2014

15. Y. Shen, D. Jacobs, G. Malliaras, G. Koley, M. Spencer, and A. Ioannidis, "Modification of indium tin oxide for improved hole injection in organic light emitting diodes," Adv. Mater. **13**(16), 1234–1238 (2001).
16. J.-M. Moon, J.-H. Bae, J.-A. Jeong, S.-W. Jeong, N.-J. Park, H.-K. Kim, J.-W. Kang, J.-J. Kim, and M.-S. Yi, "Enhancement of hole injection using ozone treated Ag nanodots dispersed on indium tin oxide anode for organic light emitting diodes," Appl. Phys. Lett. **90**(16), 163516 (2007).
17. X. Cao and Y. Zhang, "Performance enhancement of organic light-emitting diodes by chlorine plasma treatment of indium tin oxide," Appl. Phys. Lett. **100**(18), 183304 (2012).
18. M. F. Lo, T. W. Ng, H. W. Mo, and C. S. Lee, "Direct threat of a UV-Ozone treated indium-tin-oxide substrate to the stabilities of common organic semiconductors," Adv. Funct. Mater. **23**(13), 1718–1723 (2013).
19. P. K. Ho, J.-S. Kim, J. H. Burroughes, H. Becker, S. F. Li, T. M. Brown, F. Cacialli, and R. H. Friend, "Molecular-scale interface engineering for polymer light-emitting diodes," Nature **404**(6777), 481–484 (2000).
20. C. Qiu, Z. Xie, H. Chen, M. Wong, and H. S. Kwok, "Comparative study of metal or oxide capped indium-tin oxide anodes for organic light-emitting diodes," J. Appl. Phys. **93**(6), 3253–3258 (2003).
21. C.-W. Chu, S.-H. Li, C.-W. Chen, V. Shrotriya, and Y. Yang, "High-performance organic thin-film transistors with metal oxide/metal bilayer electrode," Appl. Phys. Lett. **87**(19), 193508 (2005).
22. Z. Wang, M. Helander, M. Greiner, J. Qiu, and Z. Lu, "Analysis of charge-injection characteristics at electrode-organic interfaces: Case study of transition-metal oxides," Phys. Rev. B **80**(23), 235325 (2009).
23. H. Aziz, Z. D. Popovic, N.-X. Hu, A.-M. Hor, and G. Xu, "Degradation mechanism of small molecule-based organic light-emitting devices," Science **283**(5409), 1900–1902 (1999).
24. M. de Jong, L. Van Ijzendoorn, and M. De Voigt, "Stability of the interface between indium-tin-oxide and poly (3, 4-ethylenedioxythiophene)/poly (styrenesulfonate) in polymer light-emitting diodes," Appl. Phys. Lett. **77**(14), 2255–2257 (2000).
25. X. Zhi, G. Zhao, T. Zhu, and Y. Li, "The morphological, optical and electrical properties of SnO_2: F thin films prepared by spray pyrolysis," Surf. Interface Anal. **40**(2), 67–70 (2008).
26. D. H. Zhang and H. L. Ma, "Scattering mechanisms of charge carriers in transparent conducting oxide films," Appl. Phys. Adv. Mater. **62**(5), 487–492 (1996).
27. Y. Yang, Y. J. Zhang, X. D. Liu, and Z. Q. Li, "Influence of Coulomb interaction on the electrical transport properties of ultrathin Al:ZnO films," Appl. Phys. Lett. **100**(26), 262101 (2012).
28. A. Takagi, K. Nomura, H. Ohta, H. Yanagi, T. Kamiya, M. Hirano, and H. Hosono, "Carrier transport and electronic structure in amorphous oxide semiconductor, a-InGaZnO4," Thin Solid Films **486**(1–2), 38–41 (2005).
29. A. Andersson, N. Johansson, P. Bröms, N. Yu, D. Lupo, and W. R. Salaneck, "Fluorine tin oxide as an alternative to indium tin oxide in polymer LEDs," Adv. Mater. **10**(11), 859–863 (1998).
30. M. T. Greiner and Z. H. Lu, "Thin-film metal oxides in organic semiconductor devices: their electronic structures, work functions and interfaces," NPG Asia Mater. **5**(7), e55 (2013).
31. E. Burstein, "The anomalous optical absorption limit in InSb," Phys. Rev. **93**(3), 632–633 (1954).
32. T. S. Moss, "The interpretation of the properties of indium antimonide," Proc. Phys. Soc. London Sect. B **67**(10), 775–782 (1954).

1. Introduction

Transparent conductive oxide (TCO) films are important components of photoelectronic devices, which convert electrons to photons and/or *vice versa*, such as liquid crystal displays, organic light-emitting diodes (OLEDs), and organic solar cells (OSCs) [1–4]. Current commercial TCO thin films include indium tin oxide (ITO) and fluorine-doped tin oxide (FTO) films. In OLEDs, it is very important to match the energy level of the highest occupied molecular orbital (HOMO) of the neighboring layer of organic material and the work function (WF) of the TCO anode to optimize the organic/electrode interface for effective hole injection [5–7]. As transparent electrodes, most TCOs and emerging metallic nanostructures possess WFs in the range of 4-5 eV [8,9]. Unfortunately, the common hole transport and injection materials in OLEDs such as N,N'-bis(naphthyl)-N,N'-diphenyl-1,1'-biphenyl-4,4'-diamine (HOMO of 5.2 eV), phthalocyanine copper (II) (HOMO of 5.3 eV), 4,4',4"-tris(N-2-naphthyl-N- phenyl-amino)triphenylamine (HOMO of 5.1 eV) have higher HOMO levels than the WFs of common TCOs [10,11]. The resulting inevitable barrier at the organic/electrode heterojunction interface leads to inefficient hole injection, and consequently poor device performance [12–15].

A universal route to address this issue is to enhance the WF of TCO films, such as post-processing of ITO anodes. For example, oxidized or chlorinated ITO is well-recognized direct method to modify the WF of ITO, and involves treatment with ultraviolet/ozone or oxygen/chlorine plasma [12,16,17]. However, the treatment of ITO can reduce the stability of

#200209 - $15.00 USD Received 25 Oct 2013; revised 1 Feb 2014; accepted 16 Feb 2014; published 21 Feb 2014

common organic semiconductors [18]. Addition of surface-modified organic or inorganic layers is an alternative approach to modulate the WF of TCOs [19–22]. However, each additional layer introduces inevitable defects at the extra heterojunction interface [23]. More seriously, some surface-modification layers like poly(3,4-ethylene dioxythiophene):poly(styrenesulfonic acid) can etch the TCO electrode surface to liberate metal and oxygen ions into the adjacent layer [24]. Overall, enhancing the WF of TCO electrodes by post-processing is only expedient at present. We have reported a TCO with inherent enhanced WF, $LaTiO_3$-doped indium oxide (ILTO), which can effectively improve the performance of OLEDs and OSCs [5]. Unfortunately, the application prospects of ILTO are restricted by the scarcity of indium because of very large demand, as for other indium-containing TCOs.

FTO is another commercial TCO that is typically prepared by spray pyrolysis, which requires a high processing temperature of up to 500 °C [25]. FTO, the cost of which is comparable to that of ITO, is usually used in dye-sensitized solar cells. Other TCO materials, for instance, Al:ZnO thin films, are much cheaper than ITO because they do not contain indium. However, their WFs are still in the range of 4–5 eV [8]. Herein, we develop a TCO film with high WF that does not contain indium, praseodymium fluoride (PrF_3)-doped tin oxide (PFTO), using ion-assisted electron beam deposition. The PTFO films show good electrical and optical features. The low processing temperature implies that PrF_3 can effectively dope F into SnO_2 and simplify the fabrication process of SnO_2-based TCO films.

2. Experimental methods

Because of the advantages of uniformity and flexibility, electron beam deposition was used instead spray pyrolysis to prepare films in this work. The melting point of PrF_3 (1395 °C) is close to that of SnO_2 (1630 °C), so PrF_3 was chosen as the source of fluoride. A mixed powder of PrF_3 and SnO_2 with proportions of PrF_3:PrF_3 + SnO_2 = 1–6 mol% was processed to form a target. The PFTO films of sample A, B, C, D, E, F, corresponding to 1–6 mol% of PrF_3 in target, were deposited on glass substrates that had been ultrasonically cleaned with acetone, ethanol and deionized water. Prior to deposition, the background pressure was evacuated to lower than 3.0×10^{-3} Pa and the glass substrate was heated to 300 °C. During film deposition, the chamber was flushed with O_2 gas to maintain the working pressure at 2.0×10^{-2} Pa. An end-Hall ion source was used to assist deposition that operating at an anode voltage of 160 V, an anode current of 2 A, and a cathode current in the range of 12-15 A. The rate of deposition, which was monitored *in situ* using a thin film deposition controller, was controlled to about 0.4 nm/s until the thickness of the film reached 150 nm. Optical transmittance spectra were measured with a spectrophotometer (UV-3101PC, Shimadzu, Japan). The carrier concentration and mobility of samples were measured by a Hall effect measurement system (HMS-3000, Ecopia, Korea). Film thickness was measured with a surface profiler (XP-1, Ambios, USA). WFs were investigated with an ambient Kelvin probe (KP Technology, UK). Atomic force microscope (AFM) examination was carried out with an AFM (SPA-9700, Shimadzu) in phase mode. X-ray diffraction (XRD) patterns were collected in a powder diffractometer (D8 Focus, Bruker, Germany). High-resolution TEM (HRTEM) image was recorded with a FEI-TECNAI G2 transmission electron microscope (TEM) operating at 200 kV. All measurements were performed in ambient air.

3. Results and discussion

Figure 1 shows the conduction properties of the PFTO films, along with those of a 500 nm-thick commercial FTO film for comparison. The carrier concentrations are negative values, which indicate that the PFTO films are n-type semiconductors. As shown in Fig. 1, the carrier concentrations increase with the content of PrF_3 until they reach their maximum when the target contains 3 mol% PrF_3. After that the carrier concentrations decrease slightly, and then become constant. The maximum carrier concentration of the film made using a 3 mol% PrF_3

#200209 - $15.00 USD Received 25 Oct 2013; revised 1 Feb 2014; accepted 16 Feb 2014; published 21 Feb 2014

target is -1.298×10^{20} cm^{-3}, which is the same order as that of FTO (-2.833×10^{20} cm^{-3}). The curve indicates that PrF_3 is effective for F doping of n-type SnO_2.

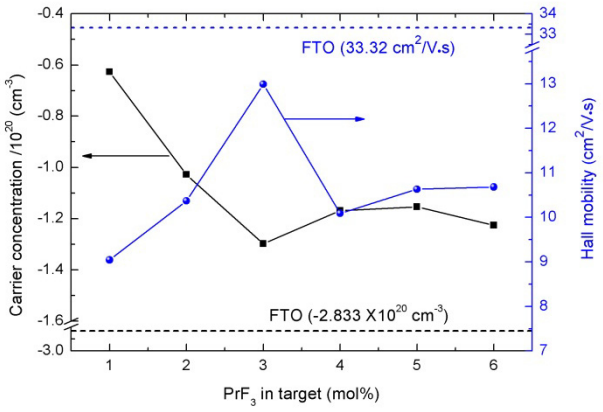

Fig. 1. Evolution of the carrier concentration and mobility of PFTO films with respect to the content of PrF_3 in the target. The blue and black dash line indicates the mobility and carrier concentration of FTO.

Figure 1 indicates that the Hall mobility of the PFTO films increases with the content of PrF_3 in the target up to 3 mol%, decreases and then remains approximately constant. The Hall mobility of the PFTO films is consistently lower than that of FTO. The factors that influence Hall mobility can be expressed as [26]:

$$\frac{1}{\mu} = \frac{1}{\mu_i} + \frac{1}{\mu_g} + \frac{1}{\mu_l} \tag{1}$$

where μ_i, μ_g and μ_l are mobilities corresponding to ionized impurities, grain boundary scattering and lattice vibrations, respectively. The surface morphology of the PFTO films are presented in Fig. 2. The grain size increases with the content of PrF_3 in the target, with grain sizes of 20, 25, 30, 35, 37 and 39 nm observed for the films deposited from targets containing 1, 2, 3, 4, 5 and 6 mol% PrF_3, respectively. The grain size of the FTO film (109 nm) is much larger than those of all of the PFTO films, and leads to its higher Hall mobility. As grain size increases, the effect of boundary scattering [26] and Coulomb interaction [27,28] weaken and lead to improved Hall mobility, as observed for the sample A, B, and C (Fig. 2). Considering the effects of impurity content, grain size and lattice vibration, it is understandable that the Hall mobility of the sample D, E, and F made from targets containing 4–6 mol% PrF_3 decrease to about 10.5 $cm^2/V{\cdot}s$. Overall, the optimal conductivity is obtained for the PFTO film grown from the 3 mol% PrF_3 target.

Figure 2 shows that the PFTO films have smaller grain size than the FTO film, but are quite flat, which is visually displayed in the section image. At the same time, the grain size of the PFTO films increases with the content of PrF_3 in the target, which affects the Hall mobility of the deposited films. The root-mean-square roughness (Rq) of the films is listed in Table 1. Because the films were deposited by electron beam deposition, the Rq of all PFTO samples is within the range from 1.1 to 2.2 nm, while that of FTO deposited by spray pyrolysis is 12.703 nm.

#200209 - $15.00 USD Received 25 Oct 2013; revised 1 Feb 2014; accepted 16 Feb 2014; published 21 Feb 2014

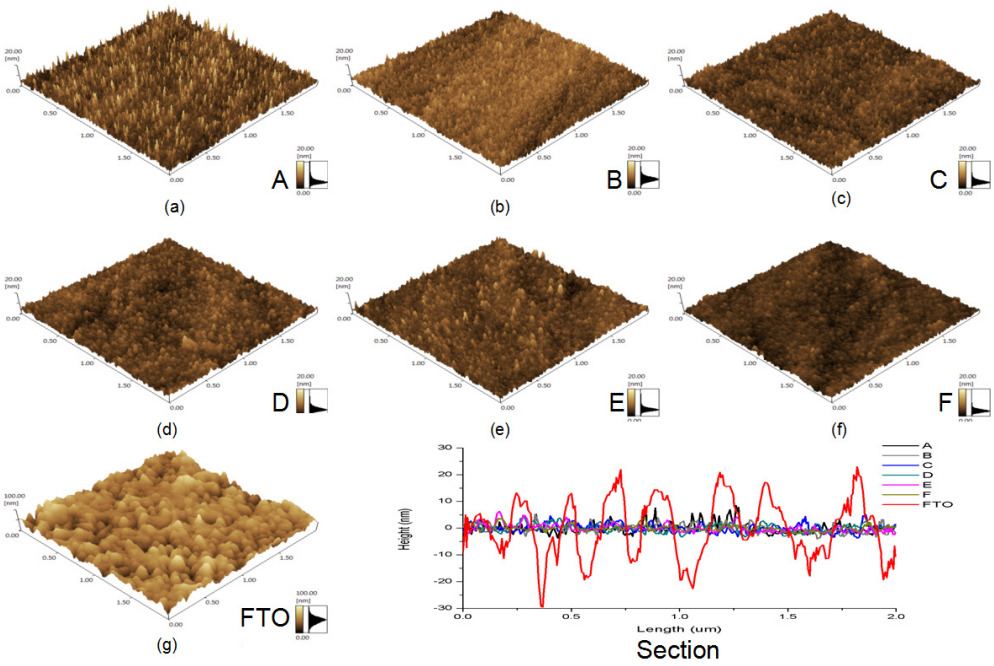

Fig. 2. Surface topography of PFTO samples in 2 × 2 μm^2 local area. The height of the PFTO and FTO films was aligned to 20 nm and 100 nm, respectively. The bottom right corner shows the height distribution for each sample. A 2-μm section of each film is shown to reveal its flatness.

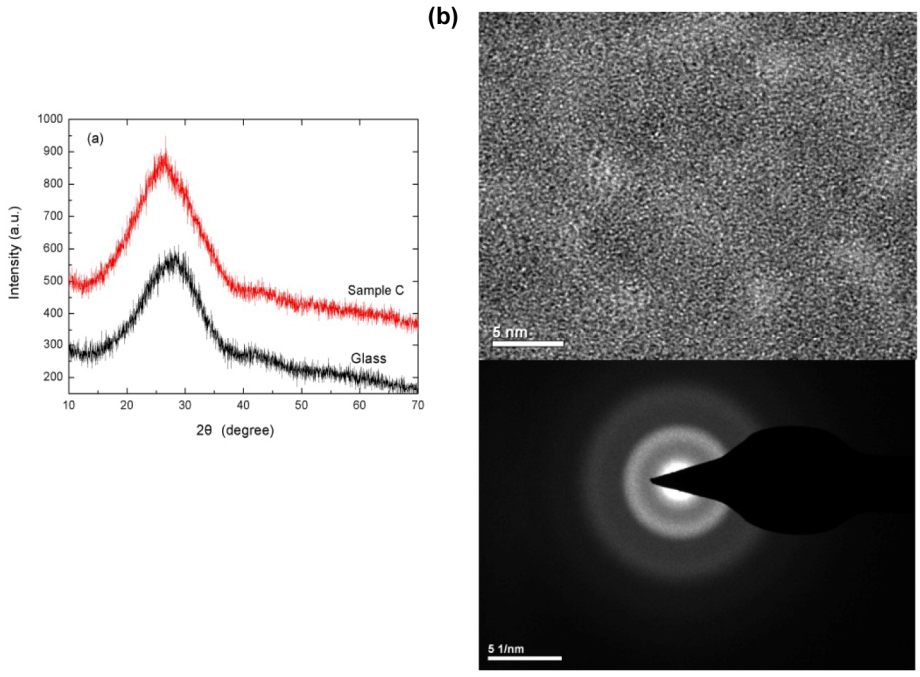

Fig. 3. (a) XRD patterns of the PFTO sample C and a glass substrate. (b) HTEM image of the PFTO film.

#200209 - $15.00 USD Received 25 Oct 2013; revised 1 Feb 2014; accepted 16 Feb 2014; published 21 Feb 2014

Table 1. The root-mean-square roughness (Rq) for different samples

Sample	FTO	A	B	C	D	E	F
Rq (nm)	12.703	2.157	1.818	1.450	1.532	1.483	1.174

The crystal structure of the PFTO samples was investigated. XRD patterns of all PFTO samples are quite similar. A typical XRD pattern of the sample C is presented in Fig. 3(a) with a weak and broad peak at 26.5°, which shows an amorphous characteristic corresponding to the (110) peak of the tetragonal rutile SnO_2 structure (JCPDS card No. 41-1445). A HRTEM image of the PFTO film confirms that the PFTO films are amorphous [Fig. 3(b)].

We conjecture that the amorphous PFTO films have a similar carrier transport mechanism to the case of amorphous oxide semiconductor $InGaZnO_4$ thin films, in which electron transport paths are made of spherical extended s orbitals [28]. Detailed conductive mechanism will be subject to further study. The WF of the PFTO films was investigated using a Kelvin probe; the results are shown in Fig. 4. Before obtaining measurements, the WF of the gold tip was calibrated with a standard gold sample with a WF of 5.15 eV. The WF of FTO films was then determined to be about 4.573 eV (average of 21 tests), which agrees with the reference values of 4.4 to 4.84 eV [29]. The same procedure was followed to investigate the WF of the PFTO films. The relationship between the WF of the film and the content of PrF_3 in the target can be fitted to a first-order curve. The negative slope shows that WF decreases with the content of PrF_3. In many cases, the work function decreases when the carrier concentration increases. While, work function is very sensitive to a number of factors such as surface roughness, exposed crystal face, surface adsorbate, the presence of impurities and the stoichiometry of a material [30]. The change in work function of different PFTO samples should be a result of the joint action of many factors.

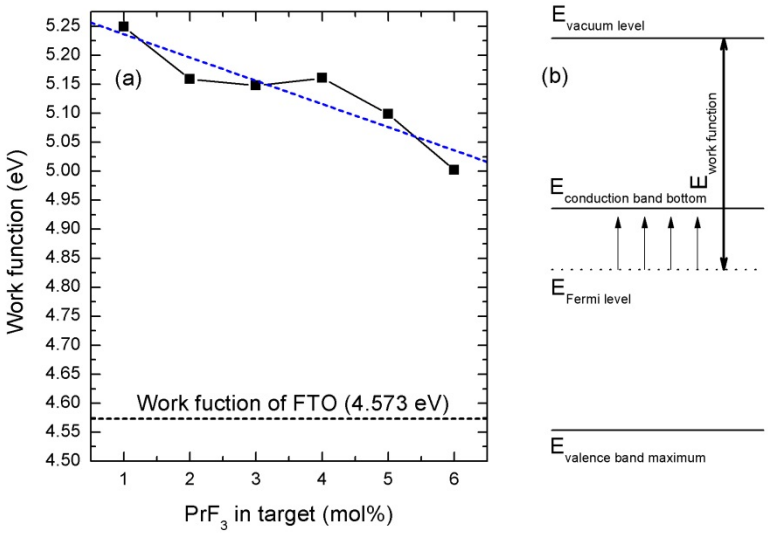

Fig. 4. (a) Dependence of the WF of PFTO films on the content of PrF_3 in the target. This relationship was fitted to a first-order curve (blue dotted line): y = 5.27662-0.04008*x, where x and y are the mole percent of PrF_3 in the target and WF, respectively. (b) An energy band model for $E_{work\ function}$. WF was defined as the energy difference between the Fermi level of the film and vacuum level.

#200209 - $15.00 USD Received 25 Oct 2013; revised 1 Feb 2014; accepted 16 Feb 2014; published 21 Feb 2014

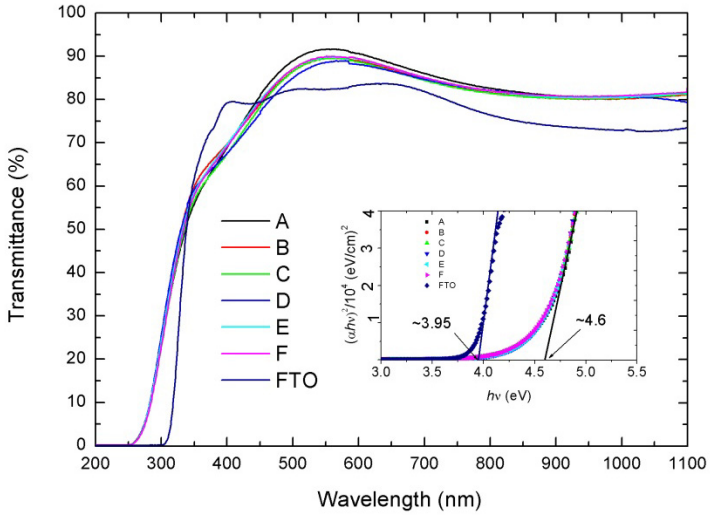

Fig. 5. Transmittance of PFTO samples and FTO. The inset shows the absorption edge.

Transmittance spectra of the PFTO samples are shown in Fig. 5. All of the PFTO films have higher average transmittance in the visible region (380–780 nm) than that of an FTO film (about 81.3%), with values ranging from 82.7% to 85.1%. All of the PFTO films show higher transmittance than that of an FTO film in the wavelength region from 480 to 1100 nm, and exhibit a peak at about 560 nm. The host material SnO_2 has a wide intrinsic band gap of 3.6 eV, and its intrinsic optical absorption edge is at about 344 nm. We determined the transmittance of the films from long to short wavelength. The transmittance suddenly drops to zero at about 314 nm for the FTO film and 260 nm for the PFTO films. That is, the optical transparency window of the PFTO films is broader than that of the FTO film, which originates from the Burstein-Moss shift effect [31, 32]. The optical band gap properties of samples were analyzed by the relation between the incident of photon energy and absorption coefficient for direct band gap semiconductor:

$$\alpha h\upsilon = A(h\upsilon - E_g)^2 \tag{2}$$

where A is a constant and α is the optical absorption coefficient, E_g is the optical bandgap energy. The inset of Fig. 5 shows that the absorption edge energy is about 3.95 eV and 4.6 eV for FTO and PFTO, respectively.

4. Conclusion

In summary, transparent conductive PFTO films were prepared by ion-assisted electron beam deposition at a low processing temperature. The PFTO films exhibited good electrical conductivity and transparency, enhanced WF and low surface roughness, suggesting that doping with PrF_3 is an effective way to dope F into SnO_2 to simplify the fabrication process of SnO_2-based TCO films. An improvement in the electrical and optical characteristics of the PFTO films might be expected by optimizing deposition parameters, annealing, and even employing other coating technologies such as magnetron sputtering, which is more suitable for mass production. Taking into account the cost of Praseodymium, PrF_3 should be replaced by a low cost fluoride in the long run.

Acknowledgments

This work was supported by the CAS Innovation Program, and the National Science Foundation of China (grant no. 61106057).